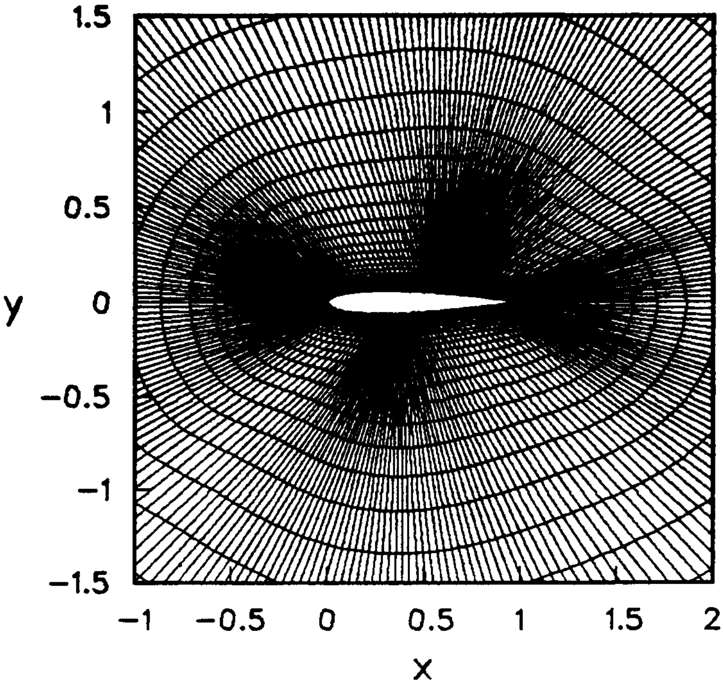

FIGURE 18. NACA0012 Mesh, 248 by 49.

11.3 Viscous Airfoils

The code ARC2D has been applied to a wide variety of viscous computations for airfoils [2], cascades [41], inlets [42], airfoils with a spoiler [43], circulation controlled airfoils [44], and others. It has been used in an unsteady mode (see the next section) and for steady viscous computations. The algorithm as presented above performs very well for viscous cases. It is convergent, fast and accurate. Two example cases are presented below. The cases are taken from the suggested problems of the 1981 Stanford Olympics [49], an RAE2822 airfoil at $M_\infty = 0.676$, $\alpha = 1.93°$, $Re = 5.7 \cdot 10^6$ and $M_\infty = 0.73$, $\alpha = 2.79$ and $Re = 6.5 \cdot 10^6$.

Results obtained from ARC2D for the first case are shown in Fig. 22. The grid used is a 248 by 51 point "O" mesh. The turbulence model was used and transition was fixed at 11% chord. Experimental data due to Cook et. al. [50] is used for comparison. We see a good comparison with experiment for pressure coefficient, and boundary layer properties.

The computed lift, drag and moment are compared with other computations and the experiment in Table 3. Due to the uncertainty of the angle of attack correction all computors matched lift. We show here our computation for both the experimentally corrected angle of attack and the values when lift is matched. Also shown are results from computors at the Stanford Olympics and some results of Mehta [51]. For the present computations at the two angles of attack the pressure

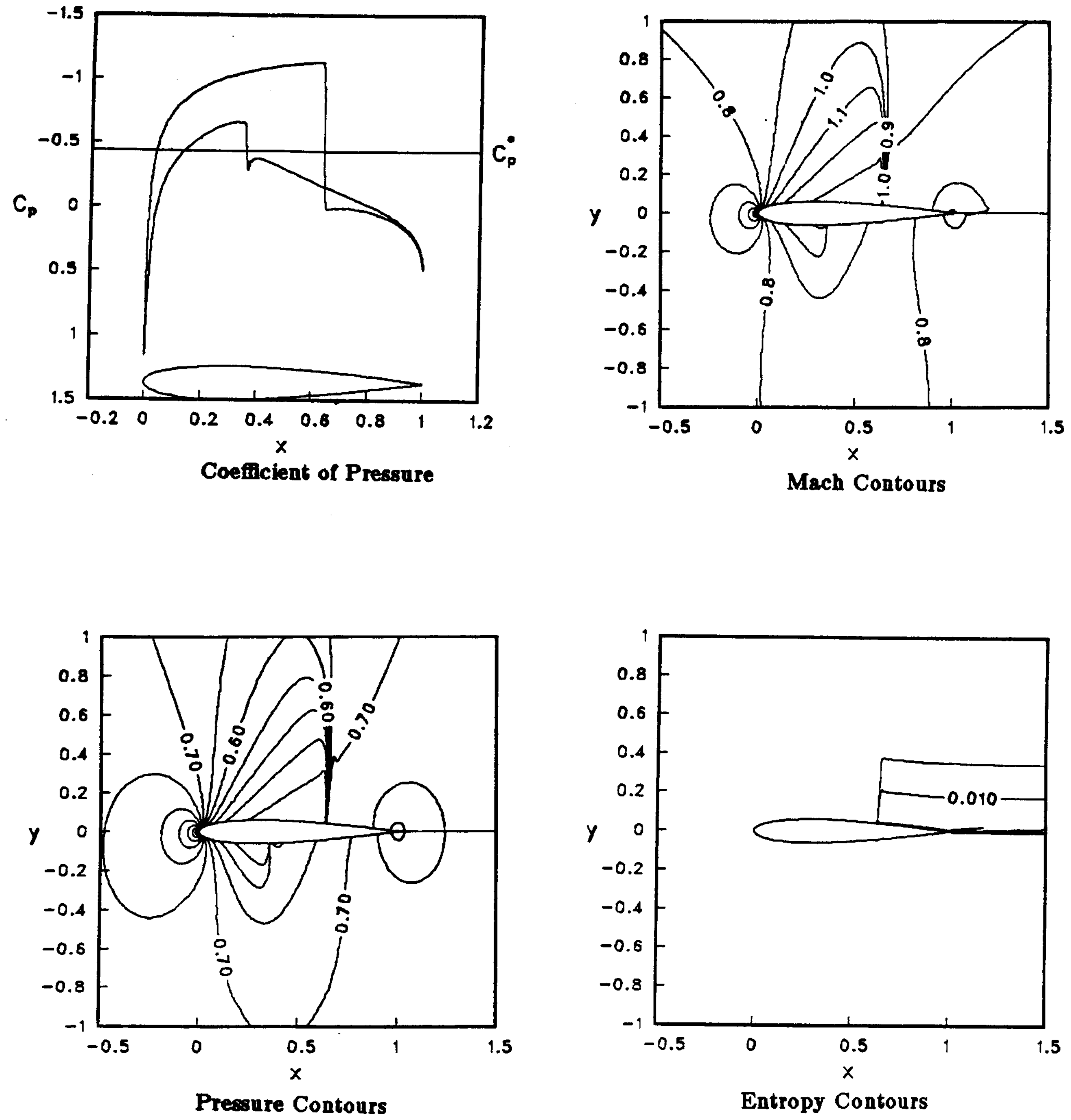

FIGURE 19. ARC2D Results for 248 by 49 Grid.

and boundary layer quantities are almost identical. The changes in lift and drag are

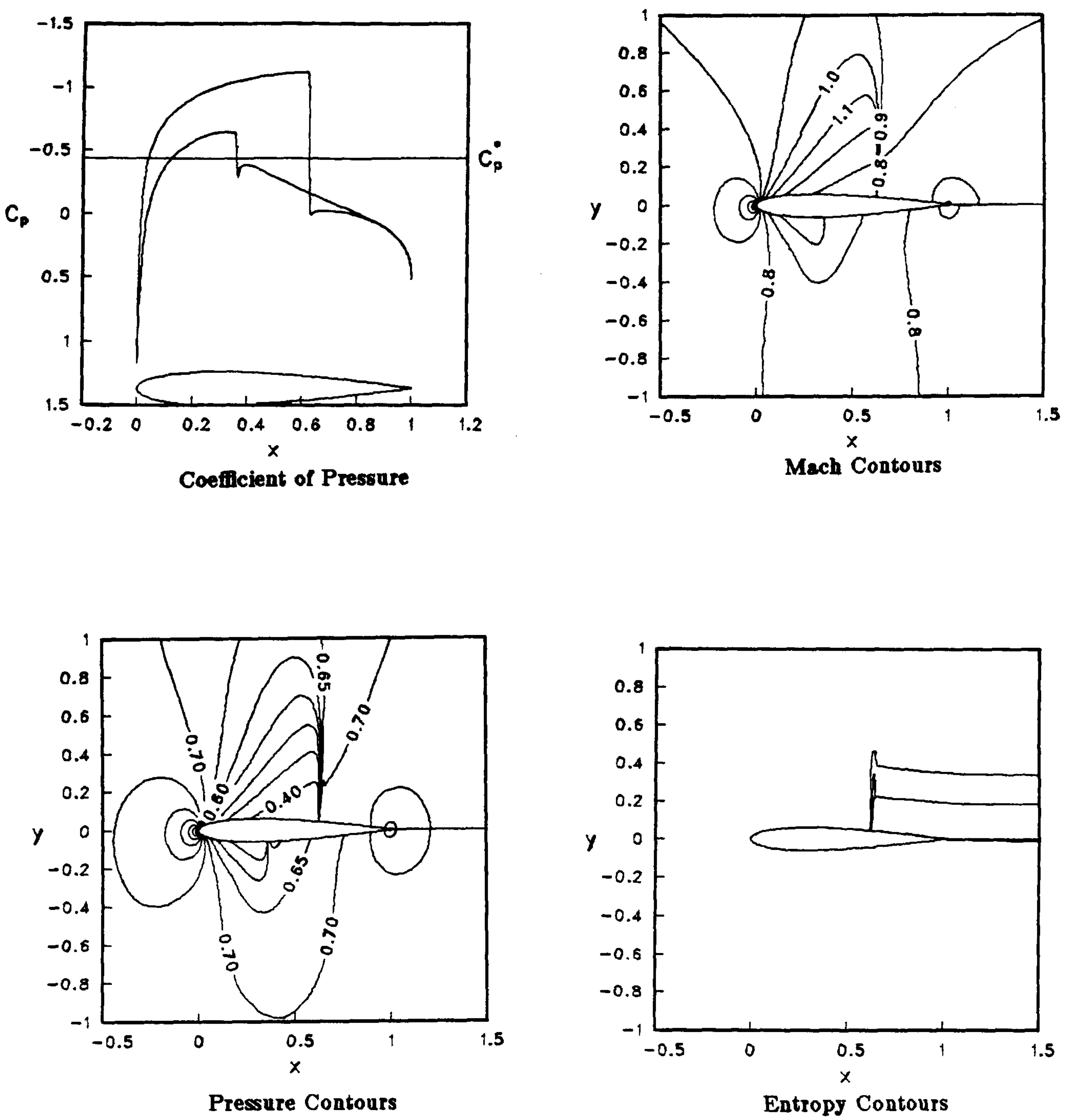

FIGURE 20. FLO52R Results for 248 by 49 Grid.

noted. The overall comparison with experiment and other computations is quite

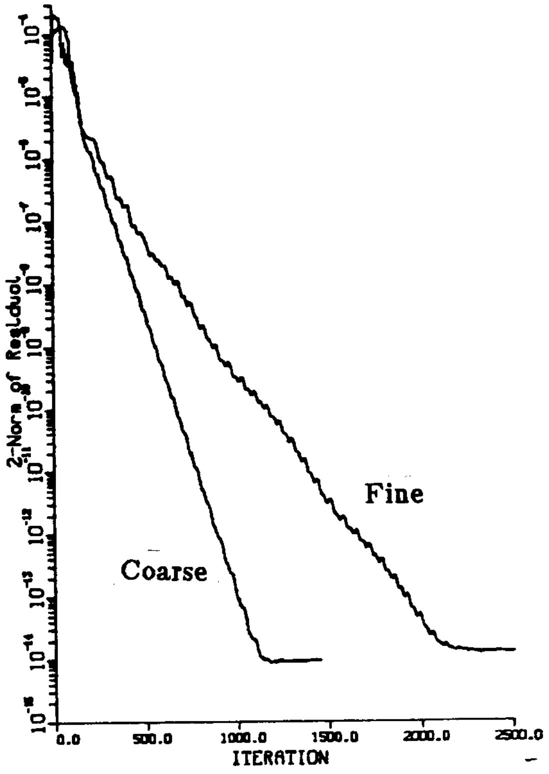

FIGURE 21. Convergence History vrs Iteration for ARC2D Results.

good.

Results obtained for the second case are shown in Fig. 23. The grid used is a 248 by 51 point "O" mesh. The turbulence model was used and transition was fixed at 3% chord. We again see a good comparison with experiment for pressure coefficient, and boundary layer properties.

The computed lift, drag and moment are compared with other computations and the experiment in Table 4. Results from computors at the Stanford Olympics and some results of Mehta [51] are shown. The overall comparison with experiment and other computations is again quite good. The shock location on the upper surface compares well. In the present computations a small region of separated flow occurs at the base of the shock and near the trailing edge on the upper surface.

Convergence history vrs iteration for these cases are shown in Fig. 24. Table 5 shows the computed convergence criteria for these cases. The convergence for these cases is quite good.

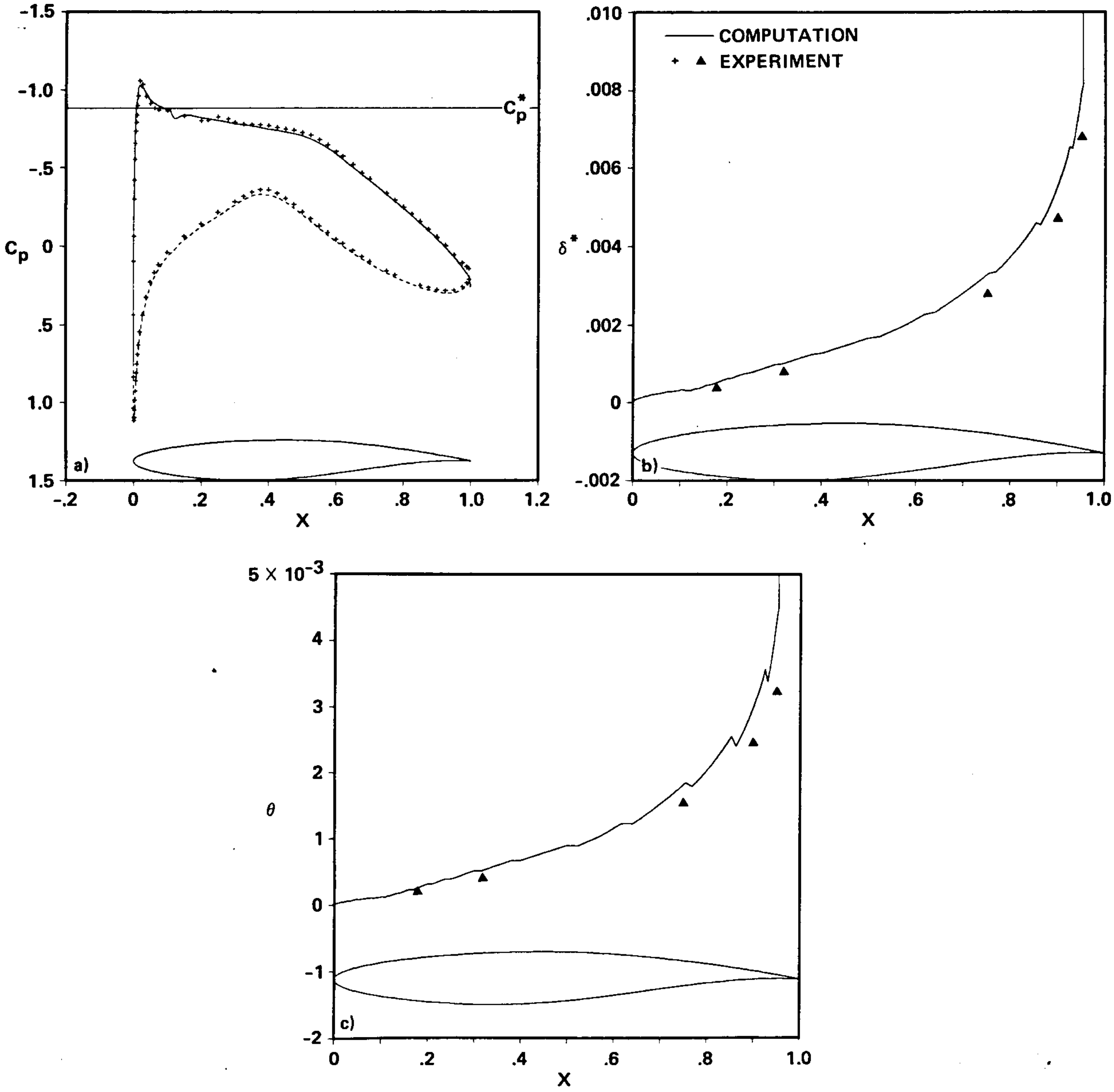

FIGURE 22. Viscous Results for RAE2822 Airfoil at $Re = 5.7 \times 10^6$, $M_\infty = 0.676$, $\alpha = 1.93°$.

11.4 Unsteady Aileron Buzz

A calculation of unsteady aileron buzz was performed by Steger and Bailey [40]. A composite of the results from their paper is shown in Fig. 25.

Loads – RAE2822 Airfoil – $M_\infty = 0.676, Re = 5.7 \times 10^6$						
	α	C_L	C_{DP}	C_{Df}	C_D	C_M
Experiment	2.40	0.566			0.0085	–0.082
Corrected Exp.	1.93	0.566			0.0085	–0.082
Mehta (1983)	1.80	0.566	0.0033	0.0061	0.0094	–0.087
Melnik (1981)	1.84	0.566	0.0027	0.0060	0.0087	–0.082
Le Balleur (1981)	1.93	0.566	0.0036	0.0056	0.0092	–0.080
Present	1.93	0.576	0.0034	0.0055	0.0089	–0.081
Present Cor. α	1.87	0.566	0.0034	0.0055	0.0089	–0.081

Table 3. Forces for RAE2822 Viscous Calculation.

In this case a two dimensional simulation of the interaction of a shock and the movable aileron (flap) on a wing was performed. Steger and Bailey used a predecessor of ARC2D coupled with a one degree of freedom equation describing the motion of the aileron on an airfoil. A airfoil with a hinge point at 75% chord was used. The aileron was free moving without damping and responded to the aerodynamic forces in balance with the inertia forces.

The flow conditions were in the transonic range of Mach number from $M_\infty = 0.76$ to 0.83 and angles of attack of $\alpha = -1.0°$ to $1.0°$. Experiments performed by Erikson and Stephenson [52] on a P-80 wing-aileron arrangement were used for comparison. A buzz boundary was established in the experiments (in terms of Mach number and angle of attack) where below the boundary the aileron remained stationary. Above the buzz boundary the shock system on the airfoil moves onto the aileron and excites the buzz motion of the aileron. An unsteady harmonic motion occurs with the upper and lower shocks running across the hinge onto and off of the aileron.

Steger and Bailey simulated this flow using the thin layer Navier Stokes equations for the conditions shown by the symbols in Fig. 25b. Figure 25c shows a case below the buzz boundary. In this case they gave the aileron an initial deflection of 4° and integrated forward in time. As seen the aileron motion damps to the neutral position of 0° deflection. Above the buzz boundary even an aileron deflection of 0° is excited to the unsteady motion. In Fig. 25d the results are compared with the measure deflection angles. In Fig. 25c the computed buzz boundary compares quite well with the measured boundary.

11.5 High Angle of Attack Airfoils

Application of the code ARC2D to the study of airfoils at high angles of attack was carried out by Barton and Pulliam [53]. In this study NACA0012 airfoil flows at

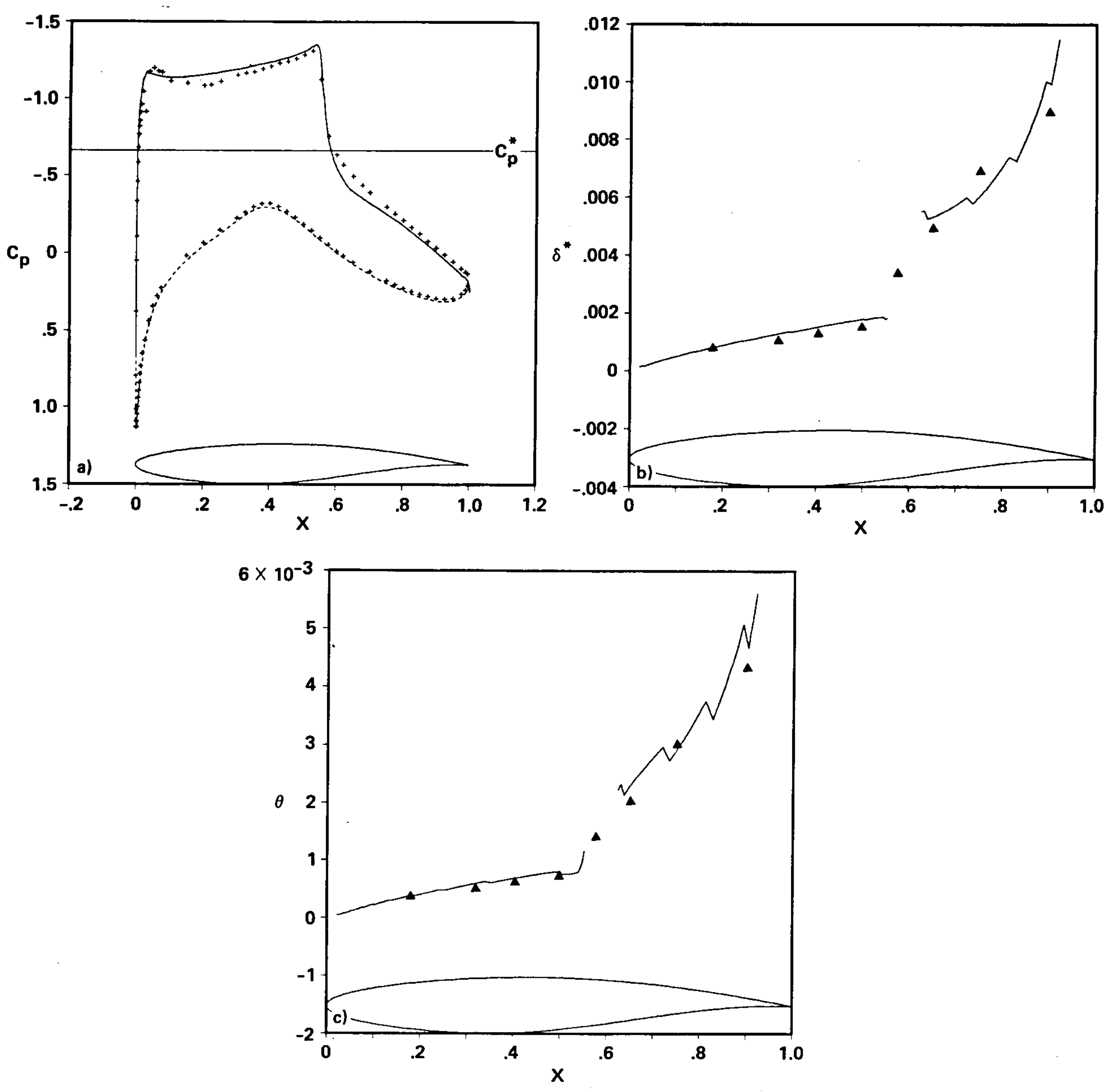

FIGURE 23. Viscous Results for RAE2822 Airfoil at $Re = 6.5 \times 10^6$, $M_\infty = 0.73$, $\alpha = 2.79°$.

low Mach number, $M_\infty = 0.25$ to 0.40 and angles of attack up to 15° were examined. Computations were performed for the Euler equations and thin layer Navier-Stokes. The calculations presented were run time accurately because unsteady effects were

Loads – RAE2822 Airfoil – $M_\infty = 0.73, Re = 6.5 \times 10^6$						
	α	C_L	C_{DP}	C_{Df}	C_D	C_M
Experiment	3.19	0.803			0.0168	–0.099
Corrected Exp.	2.79	0.803			0.0168	–0.099
Mehta (1983)	2.79	0.793	0.0118	0.0059	0.0177	–0.094
Melnik (1981)	2.54	0.803	0.0100	0.0057	0.0157	–0.094
Le Balleur (1981)	2.79	0.787	0.0111	0.0055	0.0166	–0.086
Present	2.79	0.824	0.0128	0.0050	0.0178	–0.092
Present Cor. α	2.67	0.803	0.0113	0.0051	0.0164	–0.092

Table 4. Forces for RAE2822 Viscous Calculation.

anticipated. In that paper unsteady separated but inviscid results were obtained. Comparisons were made with viscous computation and experiment to demonstrate that inviscid flow separation can be qualitatively different than viscous flow. A similar study which concentrated on comparisons with viscous experimental data was carried out by Anderson, Thomas and Rumsey [54] in which good quantitative comparison were obtained. We shall briefly discuss here the computations of Barton and Pulliam.

Barton and Pulliam presented two types of inviscid flow separation. In the first case at flow conditions, $M_\infty = 0.25 \quad \alpha = 15°$ a shock free solution with inviscid flow separation was obtained and the cause of the separation was traced to numerical error. At the high angle of attack, inaccurate boundary conditions and resolution at the leading edge produced vorticity (entropy gradients) which was convected downstream, resulting in an unsteady separation on the upper surface near the trailing edge. By refining the grid and improving the boundary conditions a steady error free solution was obtained. Figure 26 shows the entropy contours at the leading edge before and after the improvement. Figure 27 shows a comparison with full potential results using TAIR [55] and shows that good inviscid results are obtained.

At a higher Mach number $M_\infty = 0.4$ and the same angle of attack $\alpha = 15°$ a shock forms at the leading edge, see Fig. 28. In this case the shock is the source of vorticity which is then convected downstream and forms an unsteady separation. Grid refinement and the improved boundary conditions were used producing an error free leading edge, but the unsteady motion was unaffected. The vorticity (entropy) generation is a result of the strong normal shock strength gradient and high curvature of the leading edge.

The unsteady motion of the solution is depicted in Fig. 29, which shows the time history of the pressure coefficient, stream function contours and entropy fields over a complete cycle. A description of the evolution of this case is as follows. As the flow develops, a strong shock is generated at the leading edge. Entropy,

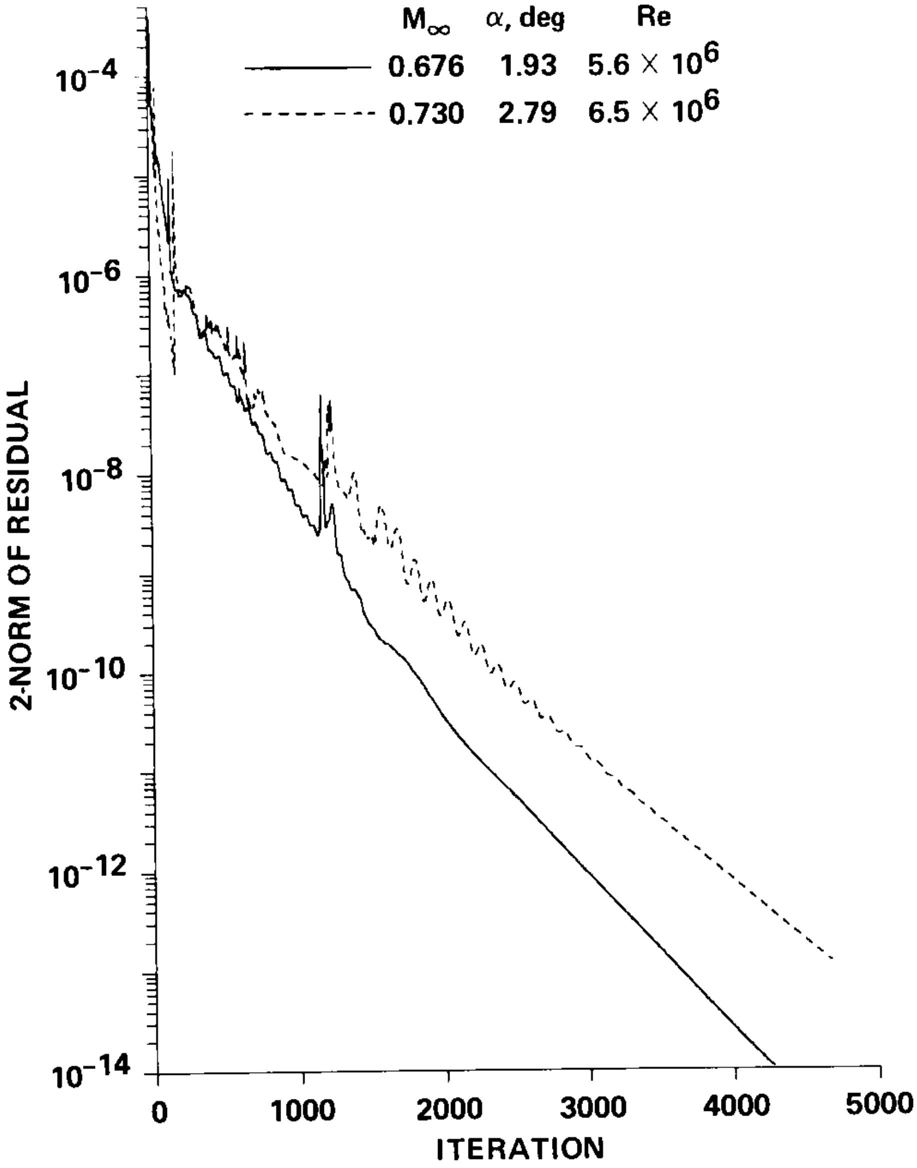

FIGURE 24. Convergence History for RAE2822 Viscous Cases.

vorticity, and pressure loss are created at the shock near the leading edge, and convected downstream along the body. A small separation region appears at the trailing edge, which grows along the body towards the leading edge. At some point the recirculation region is captured by the oncoming flow and is swept off the

Convergence Comparison (seconds)		
Criteria	$M_\infty = 0.676$	$M_\infty = 0.73$
1% of C_L	212	191
1/2% of C_L	264	295
C_L to 5 places	712	738
No. S.S. pts	608	513
Machine zero	1147	1203

Table 5. Convergence Data RAE2822 Viscous Cases.

airfoil by convection. As the recirculation region passes the trailing edge, another pocket of recirculation forms at the trailing edge, rotating in the opposite direction. This counter-rotation is caused by the flow off the lower surface, whose direction is opposite to that of the original region of recirculation. The shock then collapses, and begins to slowly grow in strength as the pattern repeats itself. This flow pattern has a well defined period and amplitude and has been reproduced in other computations with similar grids and different values of time step and artificial viscosity.

As a final case Barton and Pulliam computed a viscous calculation at similar conditions, a Mach number $M_\infty = 0.301$ and $\alpha = 13.5°$. The Reynolds number used was $Re = 3.91 \times 10^6$ and the calculation was performed using the algebraic eddy-viscosity turbulence model. In this case experimental data due to McCroskey [56] was available. For an inviscid simulation unsteady results similar to the above $M_\infty = 0.4$ case were obtained, but for the viscous computation a steady results occurred which compared well with the experimental data. The steady viscous comparison is shown in Fig. 30.

Assuming the validity of the inviscid oscillation for this case, it was concluded conclude that the Euler solution is not a good approximation to the Navier-Stokes solution, under these conditions. I refer the reader to the full paper for more details.